Comput Geosci (2012) 16:177–192
DOI 10.1007/s10596-011-9261-3

ORIGINAL PAPER

A comparison between a Monte Carlo implementation of retrospective optimal interpolation and an ensemble Kalman filter in nonlinear dynamics

Hyo-Jong Song · Gyu-Ho Lim · Baek-Min Kim

Received: 21 February 2011 / Accepted: 5 October 2011 / Published online: 9 November 2011

Abstract To more correctly estimate the error covariance of an evolved state of a nonlinear dynamical system, the second and higher-order moments of the prior error need to be known. Retrospective optimal interpolation (ROI) may require relatively less information on the higher-order moments of the prior errors than an ensemble Kalman filter (EnKF) because it uses the initial conditions as the background states instead of forecasts. Analogous to the extension of a Kalman filter into an EnKF, an ensemble retrospective optimal interpolation (EnROI) technique was derived using the Monte Carlo method from ROI. In contrast to the deterministic version of ROI, the background error covariance is represented by a background ensemble in EnROI. By sequentially applying EnROI to a moving limited analysis window and exploiting the forecast from the average of the background ensemble of EnROI as a guess field, the computation costs for EnROI can be reduced. In the numerical experiment using a Lorenz-96 model and a Model-III of Lorenz with a perfect-model assumption, the cost-effectiveness of the suboptimal version of EnROI is demonstrated to be superior to that of EnKF using perturbed observations.

Keywords Retrospective optimal interpolation · Ensemble Kalman filter · Ensemble retrospective optimal interpolation · Gaussianity · Lorenz-96 model · Lorenz model-III

H.-J. Song (✉) · G.-H. Lim
School of Earth and Environmental Sciences,
Seoul National University, Daehak-dong,
Gwanak-gu, Seoul 151-747, South Korea
e-mail: shj3777@snu.ac.kr

B.-M. Kim
Korea Polar Research Institute,
Seoul, South Korea

Present Address:
H.-J. Song
Next Generation Model Development Center,
Sindaebang 2-dong, Dongjak-gu,
Seoul 156-710, South Korea
e-mail: shj3777@gmail.com

1 Introduction

Optimal interpolation (OI) yields a variance-minimum solution by combining observation and background states at a given time. While the formulation of a Kalman filter (KF) is based on OI, the use of a forecast as a background state was derived from a time-dependent linear system [13]. If the associated system is linear, the forecast error covariance can be represented by transforming the initial error covariance with a linear system in matrix form. However, since the governing system of the atmosphere is intrinsically nonlinear, another method of estimating the forecast error covariance that is acceptable for nonlinear dynamic systems is needed in order to apply a KF to the atmosphere.

One way to implement a Kalman filter in nonlinear dynamic systems is to use an ensemble Kalman filter (EnKF) in which the forecast error covariance is replaced with a forecast ensemble covariance [7, 10, 11]. Because the forecast error covariance in nonlinear systems depends on the higher-order moments of the initial condition errors, it is intrinsically difficult to accurately estimate the forecast error covariance, even when an initial error covariance is correctly given [19].

Generally, two approaches have been used to restrict the sampling error when estimating the forecast error covariance. One method is to regulate the previously generated covariance matrix using a priori information such as the correlation distribution, which depends on the distance between the state vector grid and the observation position or the insufficient error variance that is to be inflated [3, 9].

Hamill et al. [9] demonstrated that a localization algorithm can correct the errors that originate from suspicious correlation values among the model state variables and the observed variables. As the analysis progresses, these errors cause the analysis error variance to be underestimated. Such an underestimation can be mitigated by reducing the extent of the odd correlation value with a function of the physical distance between an observation position and a model grid. However, severe localization may produce a significant imbalance in the EnKF analysis [8].

To avoid the filter divergence yielded by the underestimation, which decreases the quality of the analysis, [3] proposed a variance inflation algorithm. This algorithm expands the total variance of the forecast errors by amplifying the distinction between each ensemble member and the ensemble mean with an inflation factor before assimilating the observations. However, excessive inflation can place too much weight on the observations, which has motivated the development of an adaptive inflation algorithm [2].

Another strategy for reducing the error in estimating the forecast error covariance (namely the background error covariance) is to use a background state of which the error covariance can be more easily estimated. A method related to this approach will be outlined in this study: An earlier state instead of a forecast will be used as a background state. Such an approach simplifies the error covariance estimation exploiting limited ensemble members. Retrospective optimal interpolation (ROI) provides a mathematical framework in which a background state can be fixed at a past time [21–23]. Analogous to the extension of a KF into an EnKF, ensemble retrospective optimal interpolation (EnROI) is formulated by implementing ROI with a Monte Carlo method. It will be shown that the background ensemble covariance of EnROI better represents the error covariance of the corresponding population than the forecast ensemble covariance of an EnKF.

The disadvantages of using an EnKF rather than EnROI to represent the background ensemble covariance are described in the next section. In Section 3, the EnROI algorithm with improved efficiency is detailed. To demonstrate the advantages of EnROI, ideal experiments were carried out using a Lorenz-96 model and a Model-III of [18] under the perfect-model assumption; the results are presented in Section 4.

2 Retrospective optimal interpolation implemented with the Monte Carlo method

2.1 Ensemble Kaman filter with perturbed observations under the perfect-model assumption

In this study, the formulation of [5] is used for the EnKF. Suppose that there is an initial condition $\mathbf{x}_0^b$ at time t_0. The initial ensemble members $\mathbf{x}_0^{b(k)}$ are obtained by adding perturbations that are produced from the initial error covariance $\mathbf{B}$ to $\mathbf{x}_0^b$. Furthermore, it is assumed that a forecasting model $M_{i+1|i}(\mathbf{x}_i)$ perfectly describes the evolution of the atmosphere, namely,

$$\mathbf{x}_{i+1}^t = M_{i+1|i}\left(\mathbf{x}_i{}^t\right), \tag{1}$$

where $\mathbf{x}_i^t$ is an atmospheric state captured at model grids at time t_i. The forecast ensemble $\mathbf{x}_1^{f(k)}$ is attained by evolving the initial ensemble members $\mathbf{x}_0^{b(k)}$:

$$\mathbf{x}_1^{f(k)} = M_{1|0}\left(\mathbf{x}_0^{b(k)}\right), \tag{2}$$

where $k = 1, 2, ..., K$ is the index denoting the ensemble members. Assuming that an observation $\mathbf{y}_1^o$ satisfies a normal distribution with an error covariance $\mathbf{R}_0$, the observation ensemble $\mathbf{y}_1^{o(k)}$ is defined as

$$\mathbf{y}_1^{o(k)} = \mathbf{y}_1^o - \varepsilon_1^{o(k)}, \tag{3}$$

In Eq. 3, $\mathbf{y}_1^o$ is a given observation and $\varepsilon_1^{o(k)}$ is derived from a random sampling of the probability distribution of $\mathbf{y}_1^o - \mathbf{y}_1^t$ with a mean of zero, where $\mathbf{y}_1^t$ is a capture of an atmospheric state $\mathbf{x}_1^t$ in the observation space. The analysis ensemble of the EnKF, $\mathbf{x}_1^{a(k)}$, is obtained by assimilating the perturbed observation $\mathbf{y}_1^{o(k)}$ into each member of the forecast ensemble $\mathbf{x}_1^{f(k)}$ using the OI formulation:

$$\mathbf{x}_1^{a(k)} = \mathbf{x}_1^{f(k)} + \mathbf{P}_1^f\mathbf{H}^{\mathrm{T}}\left[\mathbf{H}\mathbf{P}_1^f\mathbf{H}^{\mathrm{T}} + \mathbf{R}_1\right]^{-1} \times \left[\mathbf{y}_1^{o(k)} - \mathbf{H}\mathbf{x}_1^{f(k)}\right]. \tag{4}$$

The forecast error covariance $\mathbf{P}_1^f$ is expressed as

$$\mathbf{P}_1^f \approx \frac{1}{K-1}\mathbf{X}_1^f\left[\mathbf{X}_1^f\right]^{\mathrm{T}}, \tag{5}$$

where the ensemble of the EnKF forecast perturbations, $\mathbf{X}_1^f$, is

$$\mathbf{X}_1^f = \left[\mathbf{x}_1^{f(1)} - \overline{\mathbf{x}_1^{f(k)}} | \cdots | \mathbf{x}_1^{f(K)} - \overline{\mathbf{x}_1^{f(k)}}\right]. \tag{6}$$

The forecast ensemble for the next analysis step is derived from the first analysis ensemble $\mathbf{x}_1^{a(k)}$:

$$\mathbf{x}_2^{f(k)} = M_{2|1}\left(\mathbf{x}_1^{a(k)}\right). \tag{7}$$

The general analysis and forecast steps of the EnKF are written as follows:

$$\mathbf{X}_i^f = \left[\mathbf{x}_i^{f(1)} - \overline{\mathbf{x}_i^{f(k)}} | \cdots | \mathbf{x}_i^{f(K)} - \overline{\mathbf{x}_i^{f(k)}}\right], \tag{8}$$

$$\mathbf{P}_i^f \approx \frac{1}{K-1}\mathbf{X}_i^f\left[\mathbf{X}_i^f\right]^{\mathrm{T}}, \tag{9}$$

$$\mathbf{x}_i^{a(k)} = \mathbf{x}_i^{f(k)} + \mathbf{P}_i^f\mathbf{H}^{\mathrm{T}}\left[\mathbf{H}\mathbf{P}_i^f\mathbf{H}^{\mathrm{T}} + \mathbf{R}_i\right]^{-1} \times \left[\mathbf{y}_i^{o(k)} - \mathbf{H}\mathbf{x}_i^{f(k)}\right], \tag{10}$$

$$\mathbf{x}_{i+1}^{f(k)} = M_{i+1|i}\left(\mathbf{x}_i^{a(k)}\right). \tag{11}$$

where the time index $i \geq 1$.

An EnKF is expected to pursue a true state in a nonlinear system better than a KF [7]. However, knowledge of only the error covariance of an initial state is insufficient for estimating the forecast error covariance in a strongly nonlinear system [19]. When the analysis ensemble perturbations are defined as

$$\delta\mathbf{x}_i^{a(k)} \equiv \mathbf{x}_i^{a(k)} - \mathbf{x}_i^t, \tag{12}$$

the error covariance of the analysis at time t_i can be defined as:

$$\mathbf{P}_i^a = \frac{1}{K-1}\sum_{k=1}^{K}\delta\mathbf{x}_i^{a(k)}\left[\delta\mathbf{x}_i^{a(k)}\right]^{\mathrm{T}} \equiv \overline{\delta\mathbf{x}_i^{a(k)}\left[\delta\mathbf{x}_i^{a(k)}\right]^{\mathrm{T}}}. \tag{13}$$

Using Eqs. 1 and 13, the sample of the forecast error at time t_{i+1} can be related to that of the analysis at t_i:

$$\begin{aligned}\delta\mathbf{x}_{i+1}^{f(k)} &\equiv \mathbf{x}_{i+1}^{f(k)} - \mathbf{x}_{i+1}^t \\ &= M_{i+1|i}\left(\mathbf{x}_i^{a(k)}\right) - M_{i+1|i}\left(\mathbf{x}_i^t\right) \\ &= M_{i+1|i}\left(\mathbf{x}_i^t + \mathbf{x}_i^{a(k)} - \mathbf{x}_i^t\right) - M_{i+1|i}\left(\mathbf{x}_i^t\right) \\ &= \mathrm{M}_{i+1|\mathrm{i}}\delta\mathrm{x}_i^{\alpha(k)} + o\left(\left|\delta\mathrm{x}_i^{\alpha(k)}\right|^2\right),\end{aligned} \tag{14}$$

where $\mathbf{M}_{i+1|i}$ is the tangent linear model of $M_{i+1|i}(\mathbf{x}_i)$. The forecast error covariance is

$$\begin{aligned}\mathbf{P}_{i+1}^f &= \overline{\delta\mathbf{x}_{i+1}^{f(k)}\left[\delta\mathbf{x}_{i+1}^{f(k)}\right]^{\mathrm{T}}} \\ &= \mathbf{M}_{i+1|i}\overline{\delta\mathbf{x}_i^{a(k)}\left[\delta\mathbf{x}_i^{a(k)}\right]^{\mathrm{T}}}\mathbf{M}_{i+1|i}^{\mathrm{T}} + O\left(\left|\delta\mathbf{x}_i^{a(k)}\right|^3\right), \\ &= \mathbf{M}_{i+1|i}\overline{\delta\mathbf{P}_i^{a(k)}}\mathbf{M}_{i+1|i}^{\mathrm{T}} + O\left(\left|\delta\mathbf{x}_i^{a(k)}\right|^3\right),\end{aligned} \tag{15}$$

The second term in Eq. 15 comes from the skewness and the higher-order moments of the probability distribution of an estimate at a prior time t_i. Such a term implies that the forecast ensemble covariance depends on the second and higher-order moments of an analysis ensemble at a prior time. In other words, it is hard to estimate the evolved ensemble covariance correctly without information on the higher-order moments of the prior ensemble. It should be noted that it is also difficult to represent the skewness and the higher-order moments of a prior estimate beyond the error covariance using the ensemble members in the large dimension of a numeric atmospheric model [26].

The expression in Eq. 15 also signifies that the ensemble evolved by a nonlinear model may become non-Gaussian even if the prior ensemble is Gaussian. When the probability distribution of a background ensemble is not Gaussian, the minimum-variance analysis is far from the most probable state. While short intervals for model integration and frequent observations support the linear growth of the forecast error, the dependency of an EnKF on such an implemented configuration may raise questions regarding the robustness of EnKF analysis when it is applied to a nonlinear dynamic system.

2.2 Ensemble retrospective optimal interpolation

To successfully carry out data assimilation with the variance-minimum approach for an atmospheric nonlinear model, we should at most preserve the linearity of the error growth. To preserve the Gaussianity of the background ensemble for nonlinear model integration, in this study, future observations are retrospectively assimilated into the past background state. Retrospective optimal interpolation (ROI) offers a suitable framework for this task [21–23]. ROI consists of the following equation set:

$$\mathbf{x}_{0|<1:i>}^a = \mathbf{x}_{0|<1:i-1>}^a + \mathbf{W}_{0|i}\left[\mathbf{y}_i^o - H_i\left(M_{i|0}\left(\mathbf{x}_{0|<1:i-1>}^a\right)\right)\right], \tag{16}$$

$$\mathbf{P}^{a}_{0|<1:i>} = \left[\mathbf{I} - \mathbf{W}_{0|i}\mathbf{H}_i\mathbf{M}_{i|0}\right]\mathbf{P}^{a}_{0|<1:i-1>}, \tag{17}$$

$$\mathbf{W}_{0|i} = \mathbf{P}^{a}_{0|<1:i-1>}\mathbf{M}^{\mathrm{T}}_{i|0}\mathbf{H}^{\mathrm{T}}_{i} \times \left[\mathbf{H}_i\mathbf{M}_{i|0}\mathbf{P}^{a}_{0|<1:i-1>}\mathbf{M}^{\mathrm{T}}_{i|0}\mathbf{H}^{\mathrm{T}}_{i} + \mathbf{R}_i\right]^{-1}, \tag{18}$$

for $i \geq 0$. Equation 16 represents the ROI analysis vector, Eq. 17 is the ROI analysis error covariance matrix, and Eq. 18 is the ROI optimal weight matrix. The subscript $0|i$ of the optimal weight matrix $\mathrm{W}_{0|i}$ means that the matrix is used to calculate the analysis increment at time t_0 by exploiting $\mathbf{y}^o_i$ at t_i. The subscript $0|<1{:}i>$ of $\mathbf{x}^a_{0|<1:i>}$ denotes the ROI analysis $\mathbf{x}^a_{0|<1:i>}$ results from the assimilation of observations, $\mathbf{y}^o_1, \ldots \mathbf{y}^o_i$ into a background state at initial time t_0. For $i = 0$, the model $M_{0|0}(\mathbf{x})$ and its derivative $M_{0|0}$ are equivalent to identities. The initial background state $\mathbf{x}^a_{0|<1:0>}$ and background error covariance $\mathbf{P}^a_{0|<1:0>}$ are equal to the given background field $\sqrt{\mathbf{e}^{\mathrm{T}}_{0|<0:n>}[\mathbf{P}^b_{0|<0:n>} - \mathbf{P}^a_{0|<0:n>}]\mathbf{e}_{0|<0:n>}}$ and the corresponding error covariance matrix $\mathbf{B}$, respectively. ROI is different from conventional OI in that it sequentially assimilates observations over the analysis window for the variance-minimum estimate of an atmospheric state $\mathbf{x}^t_0$ at t_0. Such a process is analogous to that of four-dimensional variational assimilation [15]. Note that the first analysis step of ROI is the same as in conventional optimal interpolation [14]. ROI is equivalent to the quasi-static variational assimilation process presented by [20] in that it is suitable for finding the global minimizer of its cost function [22].

Based on Eqs. 16–18, a variant of ROI can be devised using the Monte Carlo method. Hereafter, this method will be called EnROI. The analysis and forecast steps of EnROI are formulated as follows:

$$\mathbf{X}^a_{0|<1:i-1>} = \left[\mathbf{x}^{a(1)}_{0|<1:i-1>} - \overline{\mathbf{x}^{a(k)}_{0|<1:i-1>}} | \cdots | \mathbf{x}^{a(K)}_{0|<1:i-1>} - \overline{\mathbf{x}^{a(k)}_{0|<1:i-1>}}\right], \tag{19}$$

$$\mathbf{x}^{f(k)}_{i|<1:i-1>} = M_{i|0}\left(\mathbf{x}^{a(k)}_{0|<1:i-1>}\right), \tag{20}$$

$$\mathbf{X}^f_{i|<1:i-1>} = \left[\mathbf{x}^{f(1)}_{i|<1:i-1>} - \overline{\mathbf{x}^{f(k)}_{i|<1:i-1>}} | \cdots | \mathbf{x}^{f(K)}_{i|<1:i-1>} - \overline{\mathbf{x}^{f(k)}_{i|<1:i-1>}}\right], \tag{21}$$

$$\mathbf{P}^{af}_{0|i} \approx \frac{1}{K-1}\mathbf{X}^a_{0|<1:i-1>}\mathbf{X}^f_{i|<1:i-1>}, \tag{22}$$

$$\mathbf{P}^{ff}_{i} \approx \frac{1}{K-1}\mathbf{X}^f_{i|<1:i-1>}\mathbf{X}^f_{i|<1:i-1>}, \tag{23}$$

$$\mathbf{x}^{a(k)}_{0|<1:i>} = \mathbf{x}^{a(k)}_{0|<1:i-1>} + \mathbf{P}^{af}_{0|i}\mathbf{H}^{\mathrm{T}}\left[\mathbf{H}\mathbf{P}^{ff}_{i}\mathbf{H}^{\mathrm{T}} + \mathbf{R}_i\right]^{-1} \times \left[\mathbf{y}^{o(k)}_{i} - \mathbf{H}\mathbf{x}^{f(k)}_{i|<:i-1>}\right], \tag{24}$$

where $i \geq 1$. Equation 24 is used for an ROI analysis in which an observation $\mathbf{y}^o_i$ at t_i is assimilated into a previous ROI analysis $\mathbf{x}^a_{0|<1:i-1>}$ at t_0. Since a background state is fixed at initial time t_0, we expect that EnROI can eliminate the need for knowledge of the higher-order moments of a previous sample space to a some degree. However, after assimilating future observations, EnROI is affected by the nonlinearity of the employed model because the integrated state $\mathbf{x}^{f(k)}_{i|<1:i-1>}$ is used as an observation guess. In contrast to an EnKF that uses the evolved state $\mathbf{x}_i{}^{f(k)}$ as a background state, the background ensemble of EnROI will be relatively less affected. If the probability distribution of an initial ensemble is Gaussian, it can be demonstrated that EnROI preserves the Gaussianity from the initial ensemble and the observation ensemble better than the forecast ensemble of an EnKF.

EnROI is analogous to the process of four-dimensional ensemble Kalman filtering (4D-EnKF) reported by [12]. They asserted that a 4D-EnKF is equivalent to an EnKF and is advantageous in that it can assimilate asynchronous observations. We insist that the assimilation of an observation into a background at a past time can improve the quality of the analysis in addition to the assimilation of observations distributed at different times. Unlike the 4D-EnKF, EnROI maximizes these advantages by assimilating observations over an analysis window into a fixed point on the time window.

3 Implementation of EnROI

3.1 Restriction of the analysis window size

In EnROI, the period of the model integration for the forecast ensemble is overlapped in the analysis window [21]. When the analysis window and the observation interval are 24 and 6 h, respectively, the times of the model integration for EnROI are three times greater than those for EnKF. Using an EnKF with three times more ensemble members may be better than employing EnROI. Therefore, a method should be devised that enables a reduction in the computation costs for EnROI. Firstly, the analysis window size of EnROI is restricted to a finite number of observation times N

and EnROI is applied to a moving analysis window as follows:

(*Outer loop I = 0, N, 2N, ...*)

(*Inner loop n = 1, 2, ..., N*)

**EnROI step*

$$\mathbf{X}^{a}_{I|<1:I+n-1>} = \left[\mathbf{x}^{a(1)}_{I|<1:I+n-1>} - \overline{\mathbf{x}^{a(k)}_{I|<1:I+n-1>}} | \cdots \right.$$
$$\left. \cdots | \mathbf{x}^{a(K)}_{I|<1:I+n-1>} - \overline{\mathbf{x}^{a(k)}_{I|<1:I+n-1>}} \right], \quad (25)$$

$$\mathbf{x}^{f(k)}_{I+n|<1:I+n-1>} = M_{I+n|I}\left(\mathbf{x}^{a(k)}_{I|<1:I+n-1>}\right), \quad (26)$$

$$\mathbf{X}^{f}_{I+n|<1:I+n-1>} = \left[\mathbf{x}^{f(1)}_{I+n|<1:I+n-1>} - \overline{\mathbf{x}^{f(k)}_{I+n|<1:I+n-1>}} | \cdots \right.$$
$$\left. \cdots | \mathbf{x}^{f(K)}_{I+n|<1:I+n-1>} - \overline{\mathbf{x}^{f(k)}_{I+n|<1:I+n-1>}} \right], \quad (27)$$

$$\mathbf{P}^{af}_{I|I+n} \approx \frac{1}{K-1}\mathbf{X}^{a}_{I|<1:I+n-1>}\mathbf{X}^{f}_{I+n|<1:I+n-1>}, \quad (28)$$

$$\mathbf{P}^{ff}_{I+n} \approx \frac{1}{K-1}\mathbf{X}^{f}_{I+n|<1:I+n-1>}\mathbf{X}^{f}_{I+n|<1:I+n-1>}, \quad (29)$$

$$\mathbf{x}^{a(k)}_{I|<1:I+n>} = \mathbf{x}^{a(k)}_{I|<1:I+n-1>} + \mathbf{P}^{af}_{I|<1:I+n>}\mathbf{H}^{\mathrm{T}} \times \left[\mathbf{H}\mathbf{P}^{ff}_{I+n}\mathbf{H}^{\mathrm{T}} + \mathbf{R}_{I+n}\right]^{-1} \times \left[\mathbf{y}^{o(k)}_{I+n} - \mathbf{H}\mathbf{x}^{f(k)}_{I+n|<1:I+n-1>}\right], \quad (30)$$

(*End of inner loop*)

**Forecast step*

$$\mathbf{x}^{a(k)}_{I+N|<1:I+N>} \equiv \mathbf{x}^{f(k)}_{I+N|<1:I+N>} = M_{I+N|I}\left(\mathbf{x}^{a(k)}_{I|<1:I+N>}\right) \quad (31)$$

(End of outer loop)

EnROI draws information from future observations back to a past time using the correlation between ensembles of different times in $\mathbf{P}^{af}_{0|i}$. As the time interval increases, the temporal correlation decreases, but the integration time for the observation guess $\mathbf{H}\mathbf{x}^{f(k)}_{i|<1:i-1>}$ increases. This means that $\mathbf{x}^{f(k)}_{i}$ can lose its Gaussian probability distribution. If the analysis window to which EnROI is applied is too long, the background ensemble of EnROI will also have a non-Gaussian probability. For analysis accuracy, as well as reduction of computation cost, the analysis window size may need to be restricted.

3.2 Avoiding overlap of the integration period for estimating forecast error covariance in EnROI

In addition to the restriction of the analysis window size, the forecast ensemble of EnROI will be approximated by exploiting the analysis ensemble of the EnKF. To perform this task, the method of reducing computation costs for ROI reported by [21] was referenced. If the following tangent linear assumption is valid in the analysis window of EnROI,

$$\begin{aligned} & M_{I+n|I}\left(\mathbf{x}^{a(k)}_{I|<1:I+n>}\right) \\ &= M_{I+n|I}\left(\mathbf{x}^{a(k)}_{I|<1:I+n-1>} + \mathbf{x}^{a(k)}_{I|<1:I+n>} - \mathbf{x}^{a(k)}_{I|<1:I+n-1>}\right) \\ &= M_{I+n|I}\left(\mathbf{x}^{a(k)}_{I|<1:I+n-1>} + \mathbf{P}^{af}_{I|I+n}\mathbf{H}^{\mathrm{T}} \times \left[\mathbf{H}\mathbf{P}^{ff}_{I+n}\mathbf{H}^{\mathrm{T}} + \mathbf{R}_{I+n}\right]^{-1} \times \left[\mathbf{y}^{o(k)}_{I+n} - \mathbf{H}\mathbf{x}^{f(k)}_{I+n|<1:I+n-1>}\right]\right) \\ &\approx M_{I+n|I}\left(\mathbf{x}^{a(k)}_{I|<1:I+n-1>}\right) + \mathbf{M}_{I+n|I}\mathbf{P}^{af}_{I|I+n}\mathbf{H}^{\mathrm{T}} \times \left[\mathbf{H}\mathbf{P}^{ff}_{I+n}\mathbf{H}^{\mathrm{T}} + \mathbf{R}_{I+n}\right]^{-1} \times \left[\mathbf{y}^{o(k)}_{I+n} - \mathbf{H}\mathbf{x}^{f(k)}_{I+n|<1:I+n-1>}\right], \end{aligned} \quad (32)$$

it can be assumed that the forecast ensemble of EnROI is equal to the analysis ensemble of the EnKF one step before the following observation time t_{I+n} in the analysis window:

$$\mathbf{x}^{f(k)}_{I+n|<1:I+n>} \approx \mathbf{x}^{a(k)}_{I+n}, \quad (33)$$

where $\mathbf{x}^{a(k)}_{I+n}$ is the analysis ensemble of the EnKF at t_{I+n}. When Eq. 33 is used, EnROI becomes equivalent to the EnKF. To preserve the advantages of EnROI, we intend to modify the EnKF analysis ensemble so that it has the same ensemble mean as the forecast ensemble of EnROI, $M_{I+1|I}(\overline{\mathbf{x}^{a(k)}_{I|<1:I+n-1>}})$.

Obtaining the forecast ensemble mean of EnROI also requires ensemble forecasting to yield the overlapping of the model integration periods in EnROI. To avoid this computational burden, we adopt an assumption that a single forecast from the averaged state of the EnROI background ensemble is equal to that

of the EnROI forecast ensemble from the background ensemble at t_{I+n}:

$$\begin{aligned}
&\overline{M_{I+n|I}\left(\mathbf{x}^{a(k)}_{I|<1:I+n>}\right)} \\
&= \overline{M_{I+n|I}\left(\overline{\mathbf{x}^{a(k)}_{I|<1:I+n>}} + \mathbf{x}^{a(k)}_{I|<1:I+n>} - \overline{\mathbf{x}^{a(k)}_{I|<1:I+n>}}\right)} \\
&\approx M_{I+n|I}\left(\overline{\mathbf{x}^{a(k)}_{I|<1:I+n>}}\right) \\
&\quad + \mathbf{M}_{I+n|I}\overline{\left[\mathbf{x}^{a(k)}_{I|<1:I+n>} - \overline{\mathbf{x}^{a(k)}_{I|<1:I+n>}}\right]} \\
&\approx M_{I+n|I}\left(\overline{\mathbf{x}^{a(k)}_{I|<1:I+n>}}\right) \\
&\quad + \mathbf{M}_{I+n|I}\overline{\left[\mathbf{x}^{a(k)}_{I|<1:I+n>} - \overline{\mathbf{x}^{a(k)}_{I|<1:I+n>}}\right]} \\
&= M_{I+1|I}\left(\overline{\mathbf{x}^{a(k)}_{I|<1:I+n>}}\right) \qquad (34)
\end{aligned}$$

Since the variance of the analysis ensemble becomes smaller after the EnROI analysis, the validity of Eq. 34 is expected to be reinforced by the EnROI analysis [21]. Also note that it is easier for Eq. 34 to be valid when compared to Eq. 32 because the norm of $\mathbf{x}^{a(k)}_{I|<1:I+n>} - \overline{\mathbf{x}^{a(k)}_{I|<1:I+n>}}$ is smaller than that of $\mathbf{x}^{a(k)}_{I|<1:I+n>} - \mathbf{x}^{a(k)}_{I|<1:I+n-1>}$. Therefore, even when Eq. 32 is not guaranteed to be valid, we can still expect the validity of Eq. 34. Finally, the forecast ensemble of EnROI is approximately given as follows:

$$\begin{aligned}
\mathbf{x}^{f(k)_Sub}_{I+n|<1:I+n-1>} &\approx \mathbf{x}^{a(k)}_{I+n} - \overline{\mathbf{x}^{a(k)}_{I+n}} \\
&\quad + M_{I+1|I}\left(\overline{\mathbf{x}^{a(k)}_{I|<1:I+n-1>}}\right). \qquad (35)
\end{aligned}$$

We replaced the forecast ensemble in Eq. 26 with Eq. 35 so as to establish a 'suboptimal version of EnROI' (EnROI_Sub in this study). Notice that while the analysis window size is small enough for EnROI to give a more accurate analysis than the EnKF, the approximation in Eq. 35 can have a negative impact on the analysis of EnROI_Sub.

3.3 Covariance inflation

Following the work of [3], the covariance inflation in the EnKF is carried out as follows:

$$\mathbf{x}^{f(k)\_infl}_{i+1} = \alpha(\mathbf{x}^{f(k)}_{i+1} - \overline{\mathbf{x}^{f(k)}_{i+1}}) + \overline{\mathbf{x}^{f(k)}_{i+1}}, \qquad (36)$$

where α is an inflation factor. In this work, this covariance inflation method of the EnKF is adopted for EnROI. Since the analysis ensemble is used as a background ensemble in EnROI, the implementation is written as:

$$\begin{aligned}
\mathbf{x}^{a(k)_inf}_{I|<1:I+n-1>} &= \alpha\left(\mathbf{x}^{a(k)}_{I|<1:I+n-1>} - \overline{\mathbf{x}^{a(k)}_{I|<1:I+n-1>}}\right) \\
&\quad + \overline{\mathbf{x}^{a(k)}_{I|<1:I+n-1>}}, \qquad (37)
\end{aligned}$$

In EnROI_Sub, Eq. 37 is used for the inflation of the background ensemble covariance. Meanwhile, the forecast ensemble of the EnROI_Sub is not given by model integration, but by approximation Eq. 35. Thus, we need to inflate the forecast ensemble covariance obtained by exploiting Eq. 35. To accomplish this, we simply spread out $\mathbf{x}^{f(k)\_Sub}_{I+n|<1:I+n-1>}$ with the same inflation factor used for the background ensemble covariance:

$$\begin{aligned}
\mathbf{x}^{f(k)_Sub_infl}_{I+n|<1:I+n-1>} &= \alpha\left(\mathbf{x}^{f(k)_Sub}_{I+n|<1:I+n-1>} - \overline{\mathbf{x}^{f(k)_Sub}_{I+n|<1:I+n-1>}}\right) \\
&\quad + \overline{\mathbf{x}^{f(k)_Sub}_{I+n|<1:I+n-1>}}. \qquad (38)
\end{aligned}$$

In fact, a tangent linear assumption underlies Eq. 38 such that the evolution of the background ensemble into the forecast ensemble is linear.

In the practical application of EnROI_Sub, we should consider the adoption of a localization algorithm. At present, we do not have sufficient knowledge of the localization method for a temporal correlation in $\mathbf{P}^{af}_{I|I+n}$. The development of a localization method for the time lag covariance will be presented in a future study. Therefore, we restrict the scope of this study to a configuration without the use of a localization method.

3.4 EnROI_Sub in the form of ensemble transform Kalman filter

An ensemble square root filter seems more appropriate to use in this setting as these so-called 'deterministic' ensemble filters manipulate the mean in the analysis equations and have the ensemble re-sampled after each analysis step. We describe the algorithm of EnROI_Sub in the form of ensemble transform Kalman filter (ETKF; [4]):

(*Outer loop* $I = 0, N, 2N, ...$)

(*Inner loop* $n = 1, 2, ..., N$)

$$\mathbf{x}^{f(k)}_{I+n|<1:I+n-1>} = M_{I+n|I+n-1}(\mathbf{x}^{a(k)}_{I+n-1|<1:I+n-1>}), \qquad (39)$$

$$\mathbf{X}^{f}_{I+n|<1:I+n-1>} = \left[\mathbf{x}^{f(1)}_{I+n|<1:I+n-1>} - \overline{\mathbf{x}^{f(k)}_{I+n|<1:I+n-1>}} | \cdots | \mathbf{x}^{f(K)}_{I+n|<1:I+n-1>} - \overline{\mathbf{x}^{f(k)}_{I+n|<1:I+n-1>}}\right], \tag{40}$$

$$\mathbf{P}^{af}_{I|I+n} \approx \frac{1}{K-1}\mathbf{X}^{a}_{I|<1:I+n-1>}\mathbf{X}^{f}_{I+n|<1:I+n-1>}, \tag{41}$$

$$\mathbf{P}^{ff}_{I+n} \approx \frac{1}{K-1}\mathbf{X}^{f}_{I+n|<1:I+n-1>}\mathbf{X}^{f}_{I+n|<1:I+n-1>}, \tag{42}$$

$$\overline{\mathbf{x}^{a(k)}_{I|<1:I+n>}} = \overline{\mathbf{x}^{a(k)}_{I|<1:I+n-1>}} + \mathbf{P}^{af}_{I|I+n}\mathbf{H}^{\mathrm{T}}\left[\mathbf{H}\mathbf{P}^{ff}_{I+n}\mathbf{H}^{\mathrm{T}} + \mathbf{R}_{I+n}\right]^{-1} \times \left[\mathbf{y}^{o}_{I+n} - \mathbf{H}\overline{\mathbf{x}^{f(k)}_{I+n|<1:I+n-1>}}\right], \tag{43}$$

$$\mathbf{X}^{a}_{I|<1:I+n>} = \mathbf{X}^{a}_{I|<1:I+n-1>}\sqrt{\left[(K-1)\mathbf{I} + \left[\mathbf{H}_{I+n}\mathbf{X}^{f}_{I+n|<1:I+n-1>}\right]^{\mathrm{T}}\mathbf{R}^{-1}_{I+n}\mathbf{H}_{I+n}\mathbf{X}^{f}_{I+n|<1:I+n-1>}\right]^{-1}} \tag{44}$$

$$\mathbf{X}^{a}_{I+n|<1:I+n>} = \mathbf{X}^{f}_{I+n|<1:I+n-1>}\sqrt{\left[(K-1)\mathbf{I} + \left[\mathbf{H}_{I+n}\mathbf{X}^{f}_{I+n|<1:I+n-1>}\right]^{\mathrm{T}}\mathbf{R}^{-1}_{I+n}\mathbf{H}_{I+n}\mathbf{X}^{f}_{I+n|<1:I+n-1>}\right]^{-1}} \tag{45}$$

$$\overline{\mathbf{x}^{a(k)}_{I+n|<1:I+n>}} \equiv M_{I+n|I}\left(\overline{\mathbf{x}^{a(k)}_{I|<1:I+n>}}\right) \tag{46}$$

$$\mathbf{x}^{a(k)}_{I+n|<1:I+n-1>} = \overline{\mathbf{x}^{a(k)}_{I+n|<1:I+n-1>}} + \mathbf{X}^{a(k)}_{I+n|<1:I+n>}, \tag{47}$$

(*End of Inner loop*)

(*End of outer loop*)

Equations 39–47 are called as 'ETROI_Sub.' The schematic of the ETROI_Sub is shown in Fig. 1.

4 Numerical experiments

4.1 Experimental settings

The analytical ability of the EnROI and EnROI_Sub methods was compared with an EnKF using perturbed observations by conducting twin experiments. Because the localization algorithm and the model error were not considered in this study, a low-order numerical model that was assumed to have no external errors was used. The Lorenz-96 model was chosen because stable analysis solutions can be obtained without localization in the assimilation system. This model also mimics the error growth of the atmospheric general circulation model (GCM) and has been used previously to compare the ability of data assimilation methods [1, 6, 16]. The Lorenz-96 model is assumed to have 40 grid points equally spaced along a latitude circle. The equations of the model, which are integrated numerically by a fourth-order Runge–Kutta scheme, are

$$\frac{\mathrm{d}X_j}{\mathrm{d}t} = \left(X_{j+1} - X_{j-2}\right)X_{j-1} - X_j + 8, \tag{48}$$

where $j = 1, ..., 40$ denotes the longitudinal coordinates. The time step was set at $\Delta t = 0.05$ for the numerical implementation, which roughly corresponds to 6 h in GCMs [17]. The doubling time of the initial error is 2.1 days, which is similar to that of GCMs.

The model in Eq. 48 was integrated for a 5-year period starting with an arbitrary initial condition and assuming the resulting state to be a true state. Referring to [27], the initial background error covariance **B** is constructed by adding a Gaussian-distributed random error with a zero mean and a variance of 0.25 to every component of the true state in order to create 100 ensemble members. The ensemble members are then integrated over 2.5 days, which is slightly longer than the doubling time of error growth in the Lorenz-96 model, to produce a forecast ensemble. Finally, **B** is found using 100 anomaly fields obtained by subtracting the average of the ensemble members from each member. We integrate the true state corresponding to the time of **B** and denote it as $\mathbf{x}^{t}_{0}$. To ensure the robustness of the experimental results, the average of the results for over 100 realizations was taken. One hundred realizations of the initial estimate $\mathbf{x}^{b}_{0}$ were provided by adding a random noise vector with a Gaussian distribution of mean zero and covariance **B** to $\mathbf{x}^{t}_{0}$.

To ensure that the observation configuration mimicked the distribution of surface stations in the midlatitudes, we locate the observation on $j = 1, 2, ..., 15$

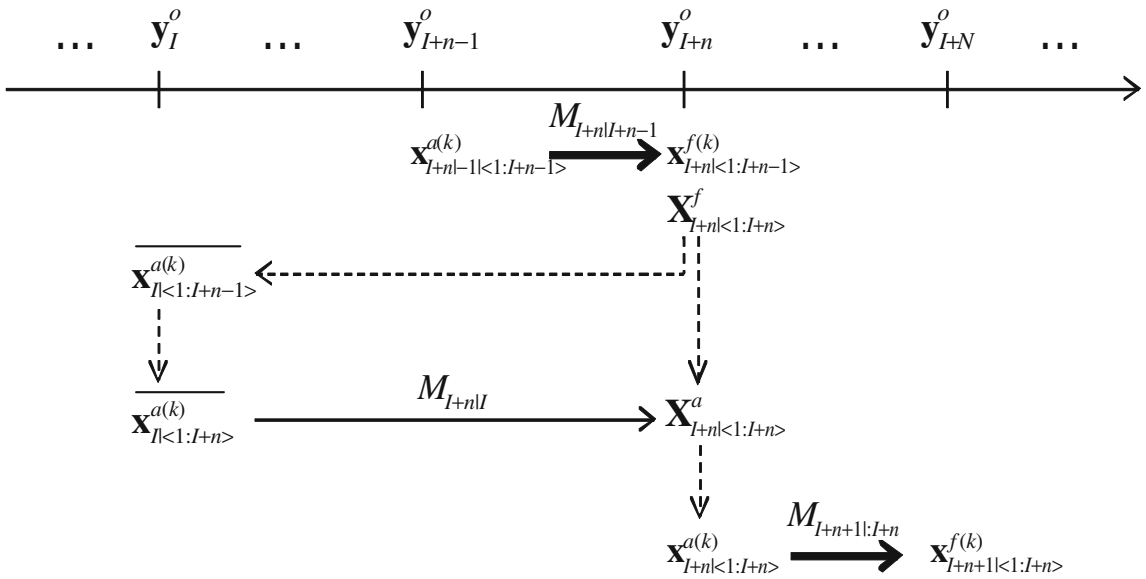

Fig. 1 A schematic diagram of ETROI_Sub in Eqs. 39–47. The *solid arrow* means that the process requires a model integration and especially the process corresponding to the *bold solid arrow* requires model integrations of which the number is equal to the number of ensemble members. The *dashed arrow* denotes that the process does not require model integrations

and $j = 21, 22, ..., 35$. Observations were distributed every 6 h by adding uncorrelated random noises with Gaussian distributions (mean = 0, variance = 0.25) to true values on the observation points. The number of observation times with a fixed time interval of 6 h is 120 from Day 0.25 (t_1) to Day 30 (t_{120}).

In the operational centers, the EnKF is applied with ensemble members smaller than the observation numbers. We use $K = 26$ ensemble members for the EnKF because it is the minimum number of members that provides stable solutions with only covariance inflation. The difference between an average of the background (observation) ensemble and a given background (observation) can unexpectedly bias the EnKF analysis. To eliminate these errors, the ensembles of background $\mathbf{x}_0^{b(k)}$ and observation $\mathbf{y}_i^{o(k)}$ were adjusted so as to guarantee that the averages of those ensembles are equivalent to the given background state and observations, respectively.

To confirm the cost-effectiveness of the reduced-rank ROI, we test our new approach on an additional model of higher dimensions than the Lorenz 40-variable model. We select the model-III of [18], which is used for comparisons of variants of ensemble Kalman filters in [24] and [22]:

$$dZ_n/dt = [X, X]_{K,n} + b^2[Y, Y]_{1,n} + c[Y, X]_{1,n} - X_n - b\,Y_n + F, \tag{49}$$

where the grid index $n = 1, ..., 120$, and the forcing $F = 15$. For any two sets of variables X and Y, $[X, Y]_{k,n}$ is defined as follows:

$$[X, Y]_{K,n} = \sum\nolimits'_{j=-J} \sum\nolimits'_{i=-J} \left(-X_{n-2K-i}Y_{n-K-j} + X_{n-K+j-i}Y_{n+K+j}\right)/K^2, \tag{50}$$

where the operator $\sum'$ denotes a modified summation, which is equal to the ordinary summation denoted by $\sum$ except that the first and last terms are to be divided by 2, and $J = K/2$. If K is odd, $J = (K-1)/2$ and $\sum'$ is replaced with $\sum$. The variable X is the sum of the longest-wave components of the control Z, and Y denotes the remaining components:

$$X_n = \sum\nolimits'_{i=-I} (\alpha - \beta\,|i|)\, Z_{n+i}, \tag{51}$$

$$Y_n = Z_n - X_n, \tag{52}$$

where α, β, and I are chosen such that X will be effectively smoothed:

$$\alpha = \left(3I^2 + 3\right)/\left(2I^3 + 4I\right), \tag{53}$$

$$\beta = \left(2I^2 + 1\right)/\left(I^4 + 2^2\right), \tag{54}$$

The coefficient b determines the frequency and amplitude of Y, and coefficient c the extent of the coupling

of X and Y. The choice of K determines the number of slow waves on the latitude circle. In this study, we set $b = 10, c = 3, K = 32, J = 16$, and $I = 12$. Equation 49 is numerically integrated by a Runge–Kutta fourth-order scheme with the time step $\Delta t = 0.001$, which is equal to 7.2 min. Settings for the assimilation experiments are the same as for the Lorenz-96 model except for observation numbers and observation time intervals; the background and observation error variances are 0.25 and the observations at each time are located on all model grids. The number of observation times with a fixed time interval of 7.2 min is 200 from 7.2 min (t_1) to 24 h (t_{200}). We use ETKF and ETROI_Sub, Eqs. 39–47, for application to the Model-III. We use $K = 33$ ensemble members for the ETKF and 30 for ETROI_Subop with 28.8-min analysis window.

4.2 Experimental results

The root-mean-squared (RMS) errors of the EnKF, Eqs. 8–11, EnROI for an analysis window size of 6 to 30 h, represented in Eqs. 25–31, are shown in Fig. 2a with different inflation factors. The EnKF produces the best analysis for an inflation factor of 1.23. With an increase in the inflation factor, the analysis quality worsens. While similar tendencies appear for EnROI, EnROI surpasses the EnKF for all of the inflation factors. Note that when the analysis window is 12 h, the analytical ability of EnROI is poor for an inflation factor of 1.23. The average over the inflation factors again shows the superiority of EnROI in terms of analysis accuracy (Fig. 2b). For an inflation factor of 1.23, the time series of the analysis RMS error confirms a more accurate analysis with EnROI (Fig. 2c). The relatively inaccurate result from EnROI, when using a 12-h analysis window, is consistent with the averaged result of Fig 1a.

To ascertain the cause of the excellent results with EnROI, the representative ability of the background ensemble covariance of the EnKF and EnROI was examined. For the EnKF, the background ensemble covariance means the forecast ensemble covariance. A score μ was defined to evaluate the representative ability of the background ensemble covariance as follows:

$$\mu = \frac{1}{K-2}\sum_{k=1}^{K-2}\left|1 - \frac{1}{100}\sum_{r=1}^{100}\frac{\varepsilon_{k,r}}{\sqrt{\lambda_{k,r}}}\right|, \tag{55}$$

where the index l is the realization number. The numerator $\varepsilon_{k,r}$ in Eq. 55 is the RMS difference between the background ensemble means of the EnKF and EnROI and the true state projected on the kth eigenvector

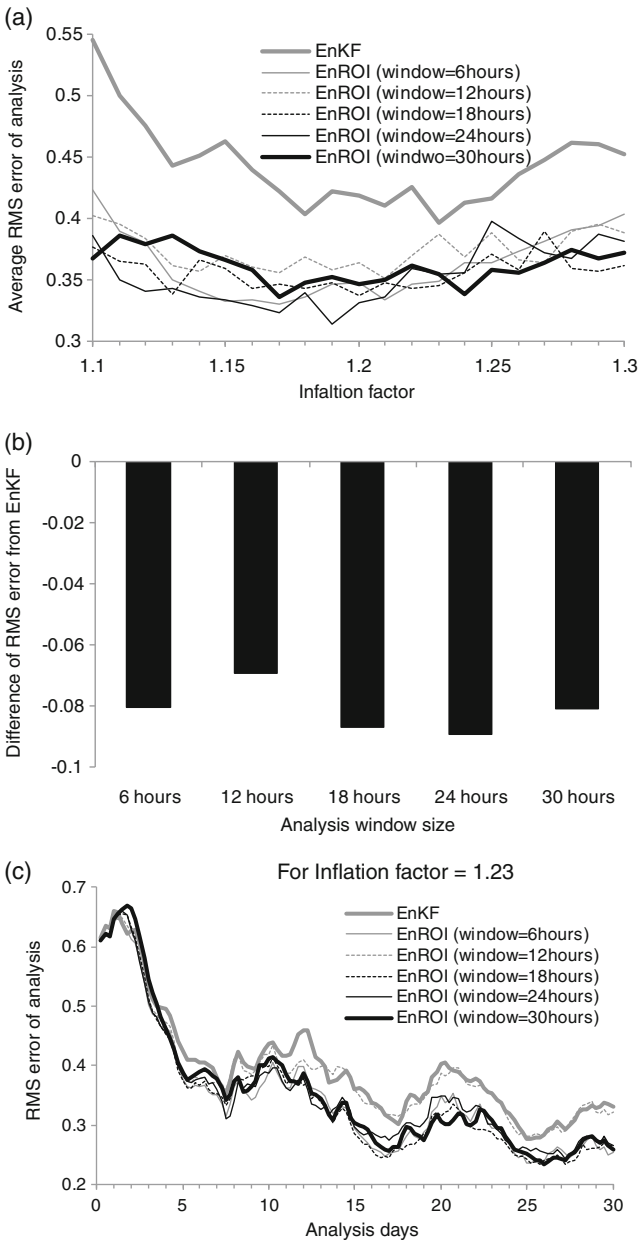

Fig. 2 **a** Average RMS errors of the analysis ensemble mean of the EnKF and the forecast ensemble mean of EnROI over the analysis days as functions of the inflation factors. The forecast ensemble of EnROI is initially evolved from the analysis ensemble of EnROI into the analysis time of the EnKF. The analysis window size of EnROI ranges from 6 to 30 h. **b** Difference in the RMS error between the EnROI analysis and the EnKF analysis averaged over the inflation factors. **c** Time series of the analysis RMS errors of the EnKF and EnROI for an inflation factor of 1.23

of the background ensemble covariance, ranked in descending order. The denominator $\lambda_{k,r}$ is the eigenvalue corresponding to the kth eigenvector. A smaller magnitude of μ indicates that the background ensemble covariance appropriately represents the RMS error of

the background state. Although the rank of the background ensemble covariance is $K-1$, sometimes the last eigenvalue is extremely close to 0. Therefore, the eigen-pairs up to $K-2$ were considered. The background ensemble covariance represents the expectation of the RMS error of the background state, not one realization. By averaging the ratio $\varepsilon_{k,r}/\sqrt{\lambda_{k,r}}$, this limitation in the evaluation of the representative ability of the ensemble covariance can be overcome. The results of the evaluation show that the background ensemble of EnROI represents the RMS errors of the background states better than that of the EnKF (Fig. 3a).

In Section 2, it was stated that an improvement in the representative ability comes from the conservation of linearity in EnROI. If this is the case, the background ensemble of EnROI should be more Gaussian than that of the EnKF. Normal probability plots of the background ensembles of the EnKF and EnROI using a 30-h analysis window show how well the background ensemble members follow a Gaussian distribution (Fig. 3b). If the data expressed with crosses follow a Gaussian distribution in the normal probability plot, the crosses lie along a straight line. The first eigenmode of the background ensemble has the most uncertainty; Gaussianity is easily lost in that eigenmode. Therefore, the probability distribution of the first eigenmode of

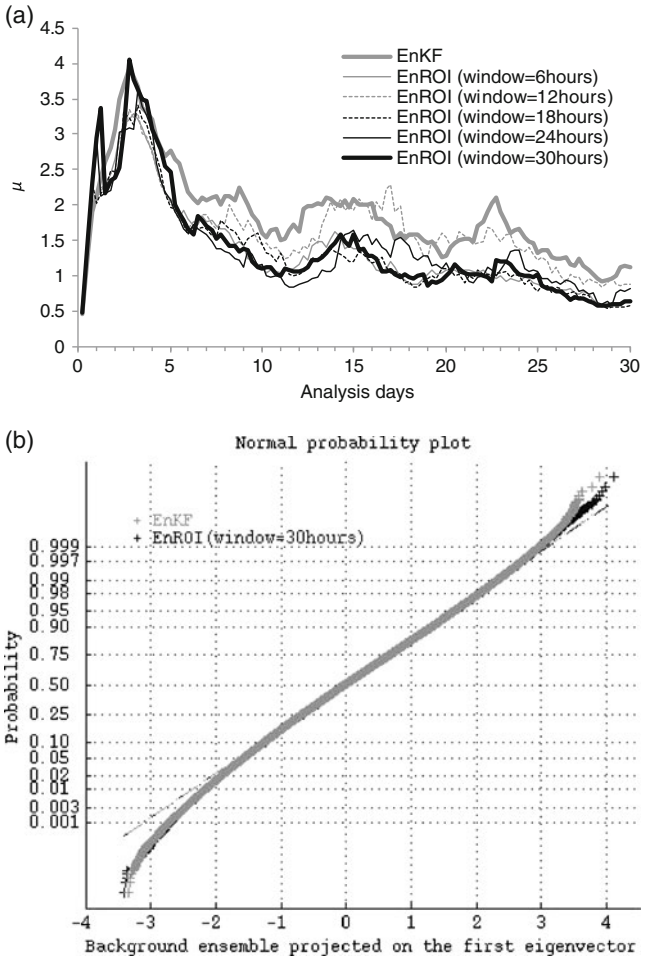

Fig. 3 **a** Representative ability of the background ensemble covariance for the EnKF and EnROI as a function of the analysis day. The representative ability is defined in Eq. 40. For the EnKF, the background ensemble means the forecast ensemble. The six curves of **a** correspond to the curves of Fig. 2c. **b** Normal probability plots for the EnKF (in *gray*) and EnROI (in *black*) using a 30-h analysis window. If the given data (*crosses*) follow a normal distribution, the *crosses lie along a straight line*. The plotted data were produced by projecting the background ensemble on its first eigenvector

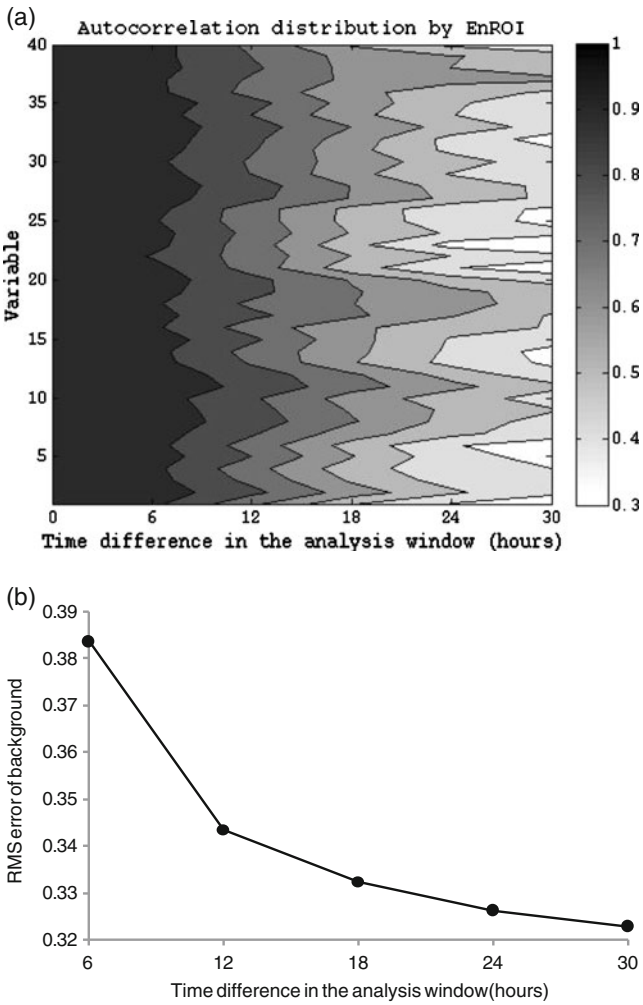

Fig. 4 **a** Autocorrelation distribution averaged over 24 composite members of EnROI using a 30-h analysis window as a function of the time difference between the initial time and the observation time over the analysis window. **b** RMS error of the background ensemble mean of EnROI at the initial time of the analysis window. The error was averaged over the 24 composite members

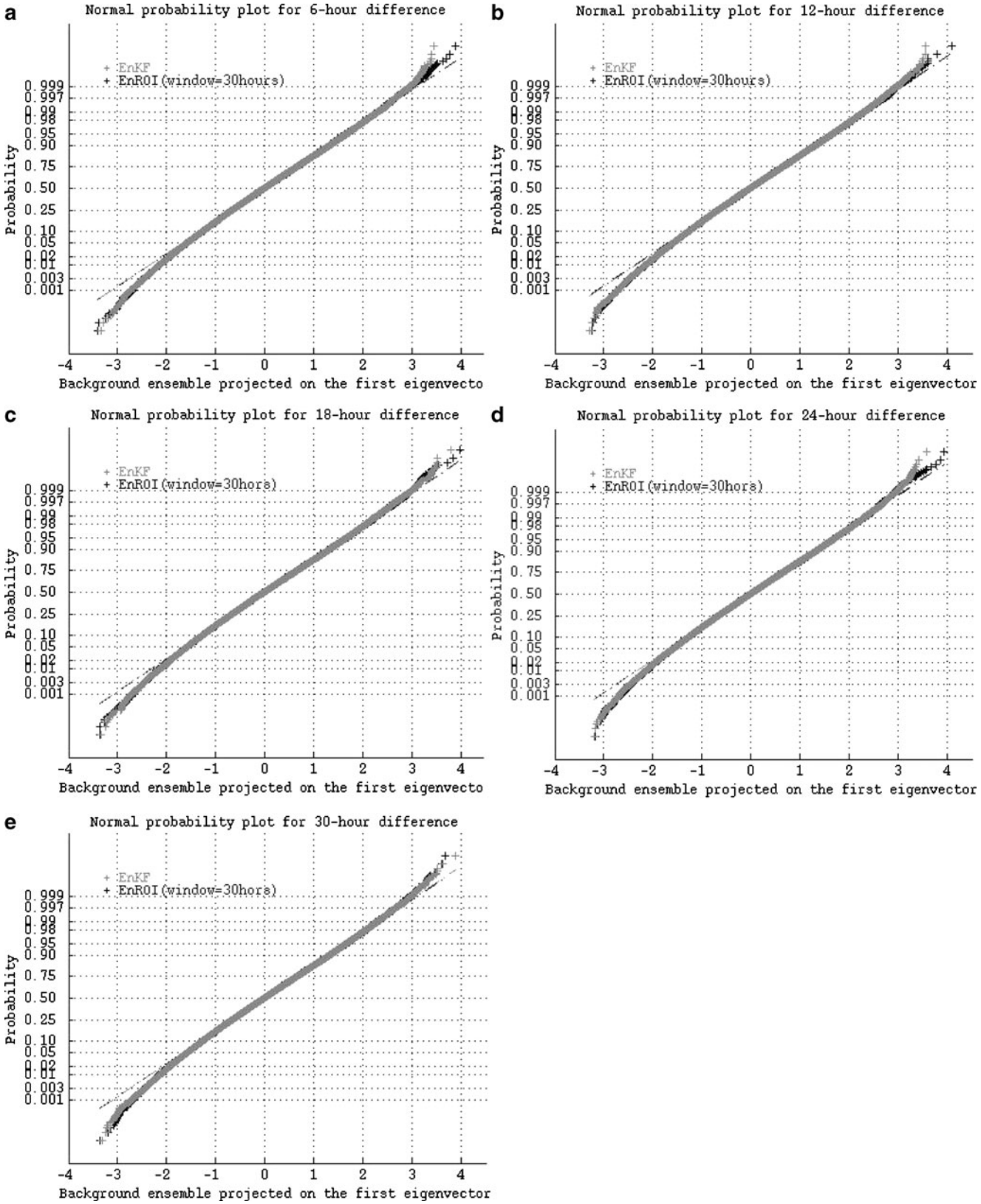

Fig. 5 Normal probability plots for the background ensembles of the EnKF and EnROI for **a** 6-, **b** 12-, **c** 18-, **d** 24-, and **e** 30-h time differences between the initial and observation times over each analysis window. The background ensemble of EnROI is at the initial time of every analysis window. The background ensemble of the EnKF means the forecast ensemble at the observation time. Samples were collected every 30 h for the 24 composite members

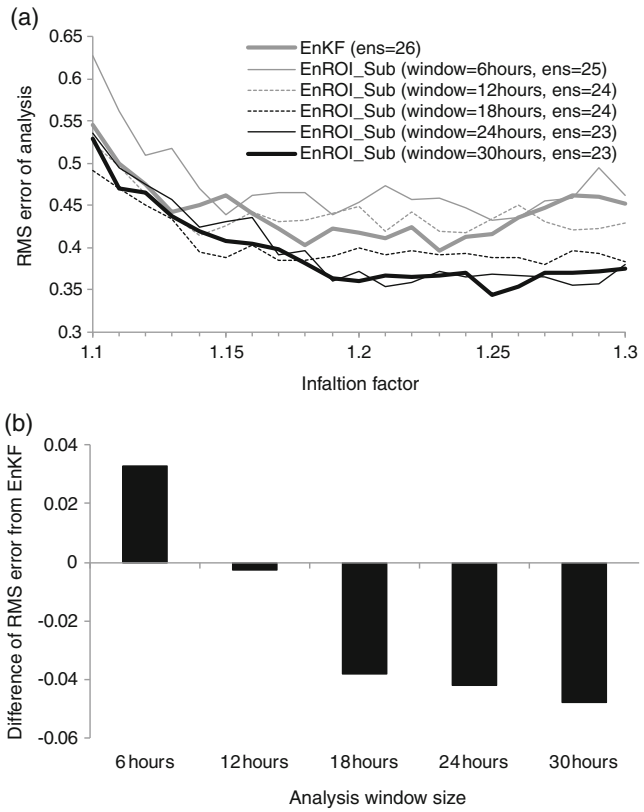

Fig. 6 **a** Average RMS errors for the analyses of the EnKF and EnROI_Sub over the analysis days as a function of the inflation factor. As in Fig. 2, the analysis window of EnROI_Sub varies from 6 to 30 h. To equate the computation costs of EnROI_Sub for model integration to the EnKF case, the ensemble size of EnROI_Sub becomes smaller than that of the EnKF. **b** Difference between the RMS error of the EnROI analysis and that of the EnKF analysis averaged for all inflation factors

the background ensemble covariance from both methods was examined to evaluate the ability of conserving Gaussianity. The average was subtracted from the background ensemble over all analysis days and the anomaly fields were restricted to the first eigenvector. The restricted anomaly fields were then normalized by the root of the first eigenvalue. While the background ensemble of the EnKF exists at every analysis time, that of EnROI exists at the initial time of each moving analysis window. We can see that, in the right-side tail of Fig. 3b, the EnKF diverges farther from the straight line designating the Gaussian distribution than EnROI. This is because the background ensemble is less affected by the nonlinear operator in EnROI than in the EnKF. The result also implies that the background ensemble covariance of EnROI can represent the second moment of the sample space of the population better than the EnKF.

Note that the maximum difference between the EnKF and EnROI in terms of the averaged analysis accuracy occurs when EnROI is used with a 24-h analysis window. For EnROI with a 30-h analysis window, the correlation map between the initial background ensemble and the forecast ensemble of EnROI in the analysis window reveals the reason for this result (Fig. 4a). All variables gradually forget their own information as the time lag increases. Shown in Fig. 4b is the background RMS error corrected by EnROI with a 30-h analysis window at the initial time of the analysis window. The result was composited according to a criterion of the same time difference between the initial time and the observation time. The number of the composite member is 24. It steeply shrinks as the time of the assimilated observation gets longer. Therefore, it can be inferred that the past background has difficulty in receiving information from observations that are too far away.

To validate the above statement, a normal probability plot for the composite samples was generated (Fig. 5). We collected the first eigenmode of the background ensemble with the same time difference from the observation time in each analysis window. For EnROI with a 30-h analysis window, we have 24 composite members for each time difference. Up to a 24-h time difference, the right-side tail of the EnKF has a shape that is more non-Gaussian than that of EnROI. However, at a 30-h time difference, the probability distributions of both the EnKF and EnROI stray from a Gaussian distribution. This result supports the statement based on Fig. 4.

While EnROI exhibits better performance than the EnKF, the computation cost for model integration in EnROI is much larger than with the EnKF. The suboptimal version of EnROI (EnROI_Sub) was compared

Table 1 Selected cases to compare the EnKF with EnROI_Sub

Experiment classification	Assimilation method	Ensemble size	Inflation factor	Analysis window size	RMS error of analysis
EnKF	EnKF	26	1.23	0 h	0.397
EnROI_Sub 1	EnROI_Sub	24	1.27	18 h	0.379
EnROI_Sub 2	EnROI_Sub	23	1.21	24 h	0.353
EnROI_Sub 3	EnROI_Sub	23	1.25	30 h	0.345

Among the various results that depend on inflation factors, the cases that produce the best analysis results are selected

with the EnKF under the same computational costs for model integration. For EnROI_Sub, the ensemble size should be decreased by $(N+1)/2$, where N denotes the observation times covered by an analysis window. When the ensemble size of the EnKF is 26, the number of ensemble members of EnROI_Sub is 25 for the 6-h window, 24 for the 12- and 18-h windows, and 23 for the 24- and 30-h analysis windows. Unlike the results of EnROI (Fig. 2), the RMS error of analysis of EnROI_Sub using 6-h analysis window is larger than that of the EnKF over most of the inflation factors (Fig. 6a). This is because the ensemble size is smaller than the EnKF and the assumption detailed in Eq. 35 harms the optimality of EnROI_Sub. However, the averaged RMS error for EnROI_Sub with 18, 24, and 30-h analysis windows (Fig. 6b) exhibits significant improvements. While EnROI_Sub uses a smaller ensemble than the EnKF, EnROI_Sub surpasses the performance of the EnKF through its retrospective approach.

To examine the performance of each method in detail, the best analysis results from the EnKF and EnROI_Sub with 18, 24, and 30-h analysis windows were selected (Table 1). A comparison of the time series reveals the superior performance of EnROI_Sub (Fig. 7a). The forecast results emphasize the distinction in analytical ability (Fig. 7b). From the result attained with an 18-h analysis window, no significant improvement in the forecasting ability is observed with EnROI_Sub. When the analysis window sizes are 24 and 30 h, the forecasting ability of EnROI_Sub is superior to that of the EnKF by about 12 lead-hour even though using smaller ensemble members.

To demonstrate how EnROI_Sub outperformed the EnKF, a plot of the representative ability of the background ensemble of the EnKF and EnROI_Sub (as defined in Eq. 40 corresponding to the RMS errors of Fig. 7a was generated (Fig. 8a). It can be seen that

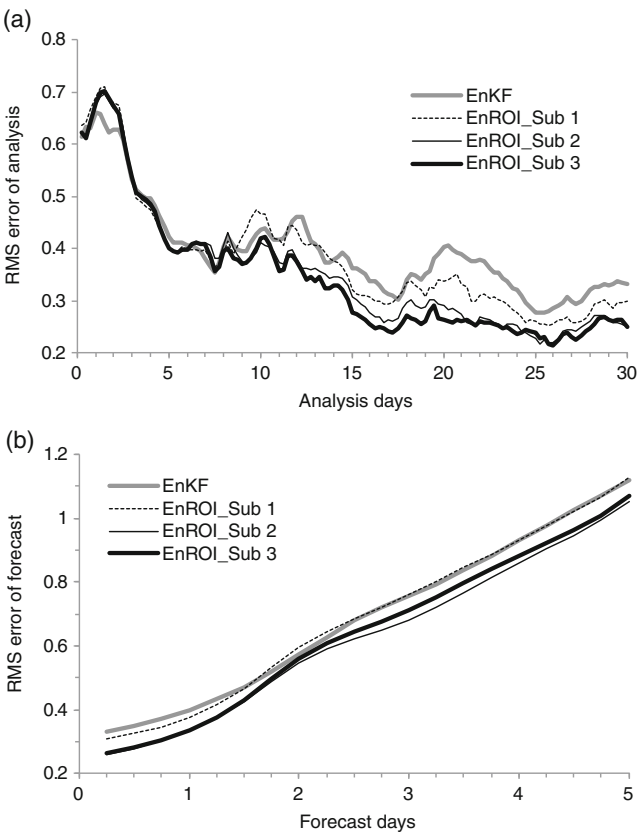

Fig. 7 **a** RMS errors of the analysis ensemble mean of the EnKF and the forecast ensemble mean of EnROI_Sub as a function of the analysis day. All *curves* correspond to the best cases of Table 1. **b** The ensemble forecast starting from the final analysis ensemble of **a**. Forecast day 0 is equal to analysis day 30 in Fig. 6

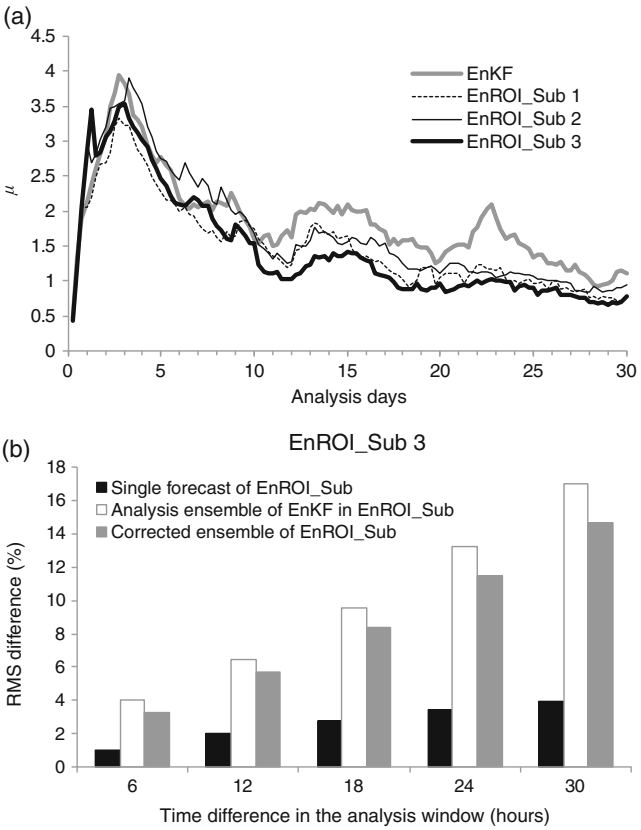

Fig. 8 **a** Representative ability of the background ensemble covariance of the EnKF and EnROI_Sub 3 as a function of the analysis day. The background ensemble covariance of the EnKF stands for the forecast ensemble covariance. **b** RMS difference between a single forecast from the average of the EnROI_Sub background ensemble at the initial time and the average of the forecast ensemble from the EnROI_Sub background ensemble (in *black*). Also shown is the RMS difference between the analysis ensemble of the EnKF (in *white*) and the forecast ensemble of EnROI_Sub adjusted with (Eq. 35; in *gray*) from the forecast ensemble from the EnROI background ensemble

the superior performance of EnROI_Sub comes from its ability to better represent the background ensemble covariance. Such a result entails that Eq. 35 is effective in approximating the forecast ensemble from the initial background ensemble. Shown in Fig. 8b is the RMS difference (black bar) between the single forecast from the initial background ensemble mean of EnROI_Sub 3 and the average of the forecast ensemble starting from the initial background ensemble of EnROI_Sub 3. The RMS difference was obtained from 24 composite members of EnROI_Sub 3 and normalized by the RMS error of the single forecast from the initial background ensemble mean of EnROI_Sub 3. The RMS difference between the analysis ensemble of the EnKF procedure in EnROI_Sub 3 (previous to correction of Eq. 35) and the forecast ensemble of the initial background ensemble is denoted with white bars. While the RMS difference of the single forecast slightly increases by less than 4% as the time difference in an analysis window increases, that of the EnKF analysis ensemble in EnROI_Sub increases by more than 16%. Such a result indicates that the validity of Eq. 34 is stronger than that of Eq. 32, as mentioned in Section 3. The RMS difference of the EnKF analysis ensemble decreases by correction of Eq. 35 (gray bar). It is thus confirmed that Eq. 35 positively works for EnROI_Sub to preserve the advantage of EnROI even though using the EnKF analysis ensemble to obtain the forecast ensemble.

As shown in Section 3.4, the EnROI_Sub has a natural description in the form of the ETKF, which we denote the ETROI_Sub, and describe by Eqs. 39–47. We compare the applications of both the ETKF and ETROI_Sub to the model-III of Lorenz. We use $K = 33$ ensemble members for the ETKF and 30 for ETROI_Subop with 28.8-min analysis window. The inflation factor for both methods is 1.25. The analysis window of ETROI_Sub is 28.8 min. Up to 6 h, the RMS error of ETKF is smaller than that of ETROI_Sub because of larger ensemble members of ETKF (Fig. 9). After 6 h, the analysis of ETROI_Sub is more stable and accurate than that of ETKF.

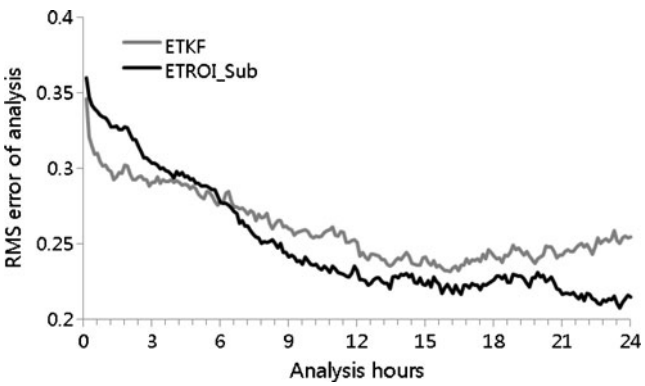

Fig. 9 Timeseries of RMS errors of the analysis ensemble mean of the ETKF and the ETROI_Sub. The analysis window of ETROI_Sub is 28.8 min. The inflation factor for both methods is 1.25

5 Summary and discussion

The KF is often seen as the gold standard of sequential data assimilation, a variance-minimum method for a nonlinear atmospheric system [14]. In this study, a different formulation known as EnROI was proposed. This formulation was motivated by the idea that, as the ensemble of an EnKF is evolved in a nonlinear system, an estimation of its covariance requires a higher-order moment of the background ensemble sample space that is not integrated by a numerical model (refer to Eq. 15). The initial background ensemble covariance is easier to represent using a restricted ensemble member size than the covariance of the evolved ensemble members.

EnROI is a variant of ROI that was implemented through the use of the Monte Carlo method. In ROI, an observation is assimilated into a past analysis state, not an evolved state [21, 23] The background ensemble of EnROI is fixed at the initial time of an analysis window. Therefore, it is expected that EnROI will yield a maximum-likelihood estimation that is better than that attained with an EnKF using only the mean and covariance without information on the higher-order moment. Because the EnROI analysis ensemble is also affected by the nonlinearity involved in obtaining the observational guess, the background ensemble is changed from a Gaussian to a non-Gaussian. However, the speed of the change can be retarded with EnROI. The numerical experiments demonstrate this phenomenon in the Lorenz-96 model with the formulation of EnKF using perturbed observations.

One must be cautious when using EnROI. Since autocorrelation between the initial analysis ensemble and the evolved ensemble decreases as the time interval between them increases, EnROI cannot obtain a significant analysis correction from observations that are too far from the analysis time. At the same time, the increase in the model integration period for the observational guess causes the background ensemble of EnROI to lose its Gaussianity. In ROI, the model integration period for obtaining the observational guess and the forecast error covariance partially overlap those of the previous analysis step [21]. The analysis window size

of EnROI needs to be restricted and EnROI must be applied to a moving analysis window with a limited size.

To reduce the computation costs of EnROI, we can use the EnKF analysis ensemble in place of the forecast ensemble of EnROI. By adjusting the analysis ensemble of the EnKF so that it had the same mean as a single forecast from the background ensemble mean of EnROI at the initial time of an analysis window, the higher accuracy of the EnROI analysis is introduced into the EnKF analysis ensemble at a future time. The modified algorithm is called suboptimal EnROI (EnROI_Sub). With the same computation costs for model integration, EnROI_Sub produced a more accurate analysis than the EnKF in numerical experiments with the Lorenz-96 model (Figs. 6 and 7).

As shown in Section 3.4, the EnROI_Sub has a natural description in the form of the ETKF, which we denote the ETROI_Sub, and describe by Eqs. 39–47. We compare the applications of both the ETKF and ETROI_Sub to the model-III of Lorenz. Up to 6 h, the RMS error of ETKF is smaller than that of ETROI_Sub because of larger ensemble members of ETKF (Fig. 9). After 6 h, the analysis of ETROI_Sub is more stable and accurate than that of ETKF.

The spread of the EnROI background ensemble decreases after it is corrected by assimilation of the observation ensemble. Therefore, the linear assumption of equality between a single forecast from the background ensemble mean of EnROI and the forecast ensemble mean from a background ensemble of EnROI (Eq. 35) is more likely to be valid than the equivalency between the analysis ensemble of the EnKF and the forecast ensemble of EnROI (Eq. 32). When 24- and 30-h analysis windows were used, the forecast ability of EnROI_Sub leads the EnKF by 12 h. Since difficulties in dealing with nonlinearity in the assimilation are inevitable with any form of an EnKF, it is expected that our result will be still applicable even when both methods are implemented using the square root forms of the EnKF [25].

We are not sure if 24- and 30-h analysis windows are suitable for a realistic model and observation configuration. Nevertheless, the theory and the numeric experimental results demonstrate the potential of EnROI_Sub as an alternative to the EnKF and promote ongoing research of the application of EnROI_Sub for practical purposes. Because of its rank deficiency, EnROI_Sub may require a localization algorithm. However, the lag covariance matrix in the EnROI_Sub formulation, $\mathbf{P}^{af}_{I|I+n}$, is not easy to localize since localization of the temporal correlation has not yet been attempted. In the numeric experiments of this study, we decided not to consider localization and simply used covariance inflation. However, the practical application of EnROI_Sub should be accompanied by the study of the localization method of correlation between model variables and observation variables at different times. This problem will be addressed in future research in a realistic setting with a complex model.

Acknowledgements We thank an anonymous reviewer for the constructive comments. G.-H. Lim was supported by the Korea Meteorological Administration Research and Development Program under grant CATER 2006–2201. B.-M. Kim was supported by Korea Meteorological Administration Research and Development Program under Grant RACS_2011-2019 (PN11020). The first author acknowledges financial support from the Brain Korea 21 Project.

References

1. Anderson, J.L.: An ensemble adjustment Kalman filter for data assimilation. Mon. Weather Rev. **129**, 2894–2903 (2001)
2. Anderson, J.L.: An adaptive covariance inflation error correction algorithm for ensemble filters. Tellus **59A**, 210–224 (2007)
3. Anderson, J.L., Anderson, S.: A Monte Carlo implementation of the nonlinear filtering problem to produce ensemble assimilations and forecasts. Mon. Weather Rev. **127**, 2741–2758 (1999)
4. Bishop, C.H., Etherton, B.J., Majumdar, S.J.: Adaptive sampling with the ensemble transform kalman filter. Part I: theoretical aspects. Mon. Weather Rev. **129**, 420–436 (2001)
5. Burgers, G., Van Leeuwen, P.J., Evensen, G.: Analysis scheme in the ensemble Kalman filter. Mon. Weather Rev. **126**, 1719–1724 (1998)
6. Descamps, L., Talagrand, O.: On some aspects of the definition of initial conditions for ensemble prediction. Mon. Weather Rev. **135**, 3260–3272 (2007)
7. Evensen G.: Sequential data assimilation with a nonlinear quasi-geostrophic model using Monte Carlo methods to forecast error statistics. J. Geophys. Res. **99**(C5), 10143–10162 (1994)
8. Hamill, T.M., Snyder, C.: Using improved background-error covariances from an ensemble Kalman filter for adaptive observations. Mon. Weather Rev. **130**, 1552–1572 (2002)
9. Hamill, T.M., Whitaker, J.S., Snyder, C.: Distance-dependent filtering of background error covariance estimates in an ensemble Kalman filter. Mon. Weather Rev. **129**, 2776–2790 (2001)
10. Houtekamer, P.L., Mitchell, H.L: Data assimilation using an ensemble Kalman filter technique. Mon. Weather Rev. **126**, 796–811 (1998)
11. Houtekamer, P.L., Mitchell, H.L., Pellerin, G., Buehner, M., Charron, M., Spacek, L., Hansen, B.: Atmospheric data assimilation with an ensemble Kalman filter: results with real observations. Mon. Weather. Rev. **133**, 604–620 (2005)
12. Hunt, B.R., Kalnay, E., Kostelich, E.J., Ott, E., Patil, D.J., Sauer, T., Szunyogh, I., Yorke, J.A., Zimin, A.V.: Four-dimensional ensemble Kalman filtering. Tellus **56A**, 273–277 (2004)

13. Kalman, R.E.: A new approach to linear filtering and prediction problems. J. Basic Eng. **82**(1), 35–45 (1960)
14. Kalnay, E.: Atmospheric Modeling, Data Assimilation and Predictability. Cambridge University Press, New York (2003)
15. Kalnay, E., Hong, L., Miyoshi, T., Yang, S.-C., Ballabrera-Poy, J.: 4-D-Var or ensemble Kalman filter? Tellus **59A**, 758–773 (2007)
16. Lorenz, E. N.: Predictability—a problem partly solved. In: Proceedings of the ECMWF Seminar on Predictability, 4–8 September 1995, Reading, England, Bol. 1, ECMWF, Shingield Park, Reading, England, pp. 1–18 (1996)
17. Lorenz, E.N., Emanuel, K.: Optimal sites for supplementary weather observations: simulation with a small model. J. Atmos. Sci. **55**, 399–414 (1998)
18. Lorenz, E.N.: Designing chaotic models. J. Atmos. Sci. **62**, 1574–1587 (2005)
19. Miller, R.N., Ghil, M., Gauthiez, F.: Advanced data assimilation in strongly nonlinear dynamical systems. J. Atmos. Sci. **51**, 1037–1056 (1994)
20. Pires, C., Vautard, R., Talagrand, O.: On extending the limits of variational assimilation in nonlinear chaotic systems. Tellus **48A**, 96–121 (1996)
21. Song, H.-J., Lim, G.-H.: An efficient retrospective optimal interpolation algorithm compared with the fixed-lag Kalman smoother by assuming a perfect model. Tellus **61A**, 610–620 (2009)
22. Song, H.-J., Lim, G.-H.: Improvement of retrospective optimal interpolation by incorporating eigen-decomposition and covariance inflation. Q. J. R. Meteorol. Soc. (2011). doi:10.1002/qj.911
23. Song, H.-J., Lim, G.-H., Lee, D.-I., Lee, H.-S.: Comparison of retrospective optimal interpolation with four-dimensional variational assimilation. Tellus **61A**, 428–437 (2009)
24. Thomas, S.J., Hacker, J.P., Anderson, J.L.: A robust formulation of the ensemble Kalman filter. Q. J. R. Meteorol. Soc. **135**, 507–521 (2009)
25. Tippett, M.K., Anderson, J.L., Bishop, C.H., Hamill, T.M., Whitaker, J.S.: Ensemble square root filters. Mon. Weather Rev. **131**, 1485–1490 (2003)
26. Van Leeuwen, P.J.: Particle filtering in geophysical systems. Mon. Weather Rev. **137**, 4089–4114 (2009)
27. Zhang, F.: Dynamics and structure of mesoscale error covariance of a winter cyclone estimated through short-range ensemble forecasts. Mon. Weather Rev. **133**, 2876–2893 (2005)